Degenerate Quasicrystal of Hard Triangular Bipyramids

Amir Haji-Akbari,[1] Michael Engel,[1] and Sharon C. Glotzer[1,2,*]

[1]*Department of Chemical Engineering, University of Michigan, Ann Arbor, Michigan 48109, USA*
[2]*Department of Materials Science and Engineering, University of Michigan, Ann Arbor, Michigan 48109, USA*

(Received 27 June 2011; published 15 November 2011)

We report a degenerate quasicrystal in Monte Carlo simulations of hard triangular bipyramids each composed of two regular tetrahedra sharing a single face. The dodecagonal quasicrystal is similar to that recently reported for hard tetrahedra [Haji-Akbari *et al.*, Nature (London) **462**, 773 (2009)] but degenerate in the pairing of tetrahedra, and self-assembles at packing fractions above 54%. This notion of degeneracy differs from the degeneracy of a quasiperiodic random tiling arising through phason flips. Free energy calculations show that a triclinic crystal is preferred at high packing fractions.

DOI: 10.1103/PhysRevLett.107.215702 PACS numbers: 64.60.Cn, 05.10.Ln, 61.44.Br, 64.60.My

Hard disks and spheres order into hexagonal and face-centered cubic crystals, respectively, above a certain packing fraction. A more complex phase behavior is observed if the disks or spheres are rigidly bonded into dimers (dumbbells) [1–4]. A solid phase, disordered in the orientation of dimers while ordered on the monomer level, forms if the distance between monomers within a dimer is roughly the diameter of a monomer. This equilibrium solid phase can be alternatively understood as a random pairing of neighboring monomers within the native monomer crystal. The resulting thermodynamic ensemble of ground states is degenerate and the structure is therefore called a degenerate crystal. As shown by Wojciechowski *et al.* [1] for hard disks, the entropy associated with the degeneracy exceeds the entropy from excluded volume effects, which by itself is sufficient to drive the crystallization of hard monomers. Other consequences of the pairing of monomers into dimers include topological defects [5], a restricted, glassy dislocation motion [6,7], and unusual elastic properties [8]. Similar degenerate phases have also been observed for freely joined chains of hard spheres [9,10].

Although degenerate crystals can potentially assemble from dimers of hard shapes other than disks and spheres, few examples have been reported. One reason is the competition between degenerate crystals and the liquid crystalline phases frequently observed for particles with large aspect ratios. For example, elongated tetragonal parallelepipeds, which for an aspect ratio of 2:1 can be viewed as dimers of face-sharing cubes, form a degenerate parquet phase at intermediate densities before transforming into a smectic liquid crystal that eventually crystallizes [11]. Another simple dimer is the triangular bipyramid (TBP), which consists of two face-sharing, regular tetrahedra [Fig. 1(a)]. The TBP is the simplest face-transitive bipyramid and the twelfth of the 92 Johnson solids. The lack of inversion symmetry of the TBP, however, makes lattice packings nonoptimal [12], and thus it is potentially more interesting as a dimer than dimers of spheres and cubes. Moreover, the recent synthesis of TBP-shaped nanoparticles and colloids [13–16] makes the investigation of this building block of practical relevance.

In both of the known ordered phases of hard, regular tetrahedra, each tetrahedron is in almost-perfect face-to-face contact with at least one other tetrahedron. The densest known packing of tetrahedra ($\phi = \frac{4000}{4671} \approx 85.63\%$) is a parallel arrangement of two dimers (four tetrahedra)—that is, two TBPs—in a triclinic unit cell to form a dimer crystal [17,18], which we refer to in the present Letter as the TBP crystal [Fig. 1(b)]. At lower packing fractions, hard tetrahedra assemble into a dodecagonal quasicrystal [19], in which the tetrahedra form a decorated square-triangle tiling [20]. Degenerate phases are impossible in the TBP crystal because the contacts between neighboring tetrahedra in different TBPs are highly imperfect [21], but are

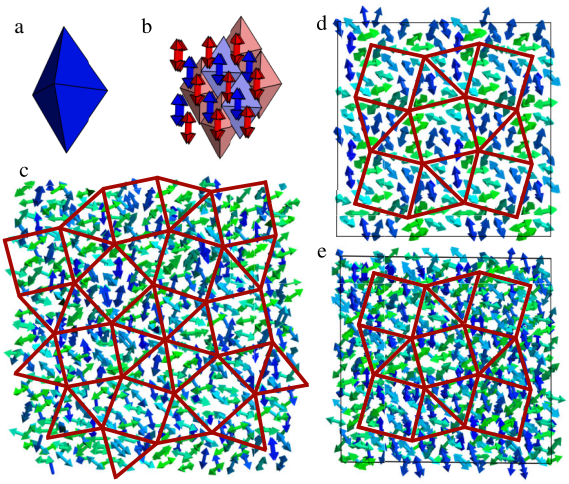

FIG. 1 (color online). Phases formed by (a) triangular bipyramids (TBPs): (b) TBP crystal, (c) degenerate quasicrystal, (d) regular quasicrystal approximant, (e) degenerate quasicrystal approximant. For visualization purposes, we show member tetrahedra of most TBPs at 30% actual size and connect their centers with bonds. In (c)–(e), tetrahedra and bonds are colored according to their orientation projected on the plane.

 © 2011 American Physical Society

possible in the quasicrystal due to the almost-perfect face-to-face contacts between all neighboring tetrahedra. Quasicrystals are solids with long-range order but without periodicity [22]. Originally discovered in metallic alloys [23], many alloy quasicrystals are now known, and a handful of quasicrystals have been reported in nonmetallic systems. Among them are quasicrystals made from spherical micelles [24], binary nanoparticles [25], and hard tetrahedra [19].

In this Letter, we investigate the phase behavior of hard TBPs and report a degenerate quasicrystal. The notion of degeneracy discussed here should not be confused with the extensively studied degeneracy associated with random tiling quasicrystals [26,27] where tiles with unique decoration patterns mix to form random tilings. We instead report a new type of randomness in the level of decorating individual tiles, in addition to the degeneracy of the random tiling.

We use isochoric and isobaric Monte Carlo (MC) simulations to study hard TBPs, which we model as perfect polyhedra with sharp vertices and edges of unit length σ. Simulations are carried out within periodic boxes with system sizes ranging from 432 to 8000 particles. Each isochoric MC cycle comprises one update per particle on average, which is either a trial translation or a trial rotation with equal probabilities. An additional box trial move is included per isobaric cycle. For fluid phases, the box is resized isotropically only, while for crystals its shape is also allowed to fluctuate. Free energies are calculated using thermodynamic integration and a modified Frenkel-Ladd method [2,28] as described in detail in [21]. Further details and simulation parameters are given in Ref. [29].

The dodecagonal quasicrystal of TBPs forms spontaneously from the equilibrium fluid phase at packing fractions above 54%. Figure 2(a) depicts a side view of the quasicrystal formed in an isobaric simulation of 2624 TBPs at reduced pressure $P^* = P\sigma^3/k_BT = 46$ and subsequently compressed to a packing fraction of 81.34%. TBPs arrange into layers (white lines), which stack on top of each other perpendicular to the twelvefold symmetry axis (dark arrow). We confirmed that the formation of the quasicrystal occurs reproducibly in systems with at least a few thousand particles and does not depend on the shape of the simulation box.

The quasicrystal structure can be best understood by replacing each bipyramid by its two member tetrahedra. Figure 2(b) depicts the centroids of tetrahedra within a few layers of Fig. 2(a). Neighboring tetrahedra are connected with bonds [30]. Dodecagons in Fig. 2(b) correspond to rings of twelve member tetrahedra, a structural motif characteristic of the quasicrystal [19]. These rings are further capped with pentagonal dipyramids (PDs), five tetrahedra sharing an edge, visible in the figure as pentagons within dodecagons. Additional member tetrahedra referred to as interstitials fill the space between the rings. Together,

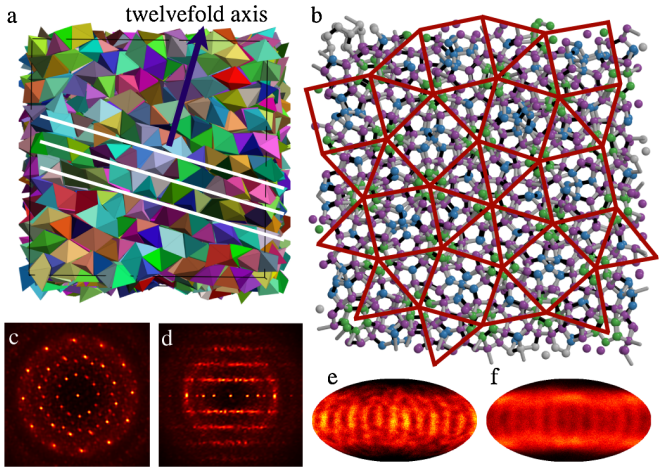

FIG. 2 (color online). (a) TBPs assemble into a dodecagonal quasicrystal in isobaric and isochoric Monte Carlo simulations. (b) The square-triangle tiling obtained by connecting the centers of twelvefold rings of member tetrahedra. Intra- and inter-TBP bonds are depicted in black and gray, respectively. (d),(e) Diffraction patterns with centers of member tetrahedra as scatterers calculated (c) perpendicular to and (d) across the layers. (e) Intra-TBP and (f) total bond order diagrams.

dodecagons and PDs form motifs whose centers are the vertices of square and triangle tiles. Their mixing gives the square-triangle tiling its overall twelvefold symmetry as observed in the diffraction pattern depicted in Fig. 2(c). Layering along the twelvefold axis can be seen in Fig. 2(d). Overall, the arrangement of the member tetrahedra is identical to that reported in the hard tetrahedron system [19].

To elucidate how the bipyramids are arranged within the quasicrystal, we compare statistical distributions of intra-TBP bonds (bonds that connect member tetrahedra within TBPs) and the set of all bonds in the quasicrystal by projecting both sets onto the surface of a unit sphere. The resulting diagrams are referred to as intra-TBP and total bond order diagrams respectively, and are visualized using the Mollweide projection with the twelvefold axis pointing in the vertical direction. Comparing these bond order diagrams [Figs. 2(e) and 2(f)], we observe no significant difference in the distribution of bond directions within the twelvefold layers. This suggests that the pairing of tetrahedra in the quasicrystal does not follow a predefined set of rules and is instead random. However, tetrahedra tend to pair more strongly within layers than between neighboring layers, a fact that can be explained by noting that face-to-face contacts are more perfect within layers. Motivated by studies of hard sphere dimers [1], we refer to the TBP quasicrystal as a degenerate quasicrystal (DQC). The randomness can be seen clearly in Fig. 1(c). It is surprising that the structural quality of the DQC is uncompromised despite the additional geometrical constraints imposed on the system by pairing tetrahedra into TBPs. For instance, we find that the maximum packing fraction achieved by replacing the bipyramids with individual

member tetrahedra and then compressing is statistically identical to that obtained in simulations of hard tetrahedra.

Approximants are periodic phases that are structurally similar to the quasicrystal locally [31]. Constructing an approximant of the TBP quasicrystal involves not only choosing a periodic tiling and decorating it with tetrahedra, but also pairing the tetrahedra into bipyramids. We choose the $(3.4.3^2.4)$ Archimedean tiling which, in the case of hard tetrahedra, gives rise to the densest approximant [19]. There is no unique way of pairing tetrahedra into TBPs even within a single unit cell of the approximant due to degeneracies associated with rotations of the capping PDs. In particular, it is not possible to avoid breaking the fourfold symmetry of the approximant unit cell in the pairing process. We constructed a regular approximant by retaining as much of the symmetry as possible. Top and bottom views of the constructed approximant are depicted in Figs. 3(a) and 3(b) while a unit cell is depicted in Fig. 3(c) where ring-ring and ring-interstitial connections are highlighted. We find that the regular approximant can be compressed to a maximum packing fraction of 83.39%, a bit less than the maximum packing fraction of 85.03% achieved for the quasicrystal approximant constructed of individual tetrahedra [19]. The distinctive difference between the intra-TBP [Fig. 3(d)] and the total bond order diagrams [Fig. 3(e)] is a result of this deterministic pairing [Fig. 1(d)].

By expanding the regular approximant, we find that it melts at $P^* \leq 35$ and packing fractions $\phi < 54\%$. But before melting, the crystal slowly transforms into a more loosely packed structure in which tetrahedra are paired at random into TBPs, just as in the DQC, although their positions and orientations are unchanged [Fig. 1(e)]. The resulting structure is therefore degenerate to the tetrahedron-based approximant and we refer to it as a degenerate approximant (DA). The angular distribution of intra-TBP bonds around the fourfold axis [Fig. 3(f)] is more similar to that of all bonds [Fig. 3(g)] in the degenerate approximant than in the case of the regular approximant [Figs. 3(d) and 3(e)], which again suggests random pairing. We find that the transformation from regular to degenerate approximant is irreversible on the time scale of our simulations ($\approx 10^8$ MC cycles). Since the DA can only be recompressed to a density of 82.88%, which is lower than the maximum density of the regular approximant, the DA has to be stabilized by its pairing disorder close to melting.

To understand how the regular approximant transforms into the DA, we note [Fig. 2(b)] that the arrangement of the member tetrahedra can be alternatively understood as a spanning network of interpenetrating PDs [19]. In the hard tetrahedron system, PDs can easily rotate around their principal axes [21]. Such rotations are also essential in understanding the local rearrangements of bipyramids at densities below 60%. As shown in Fig. 4(b), TBPs move very little at $\phi = 60\%$. Even after 250×10^6 MC cycles

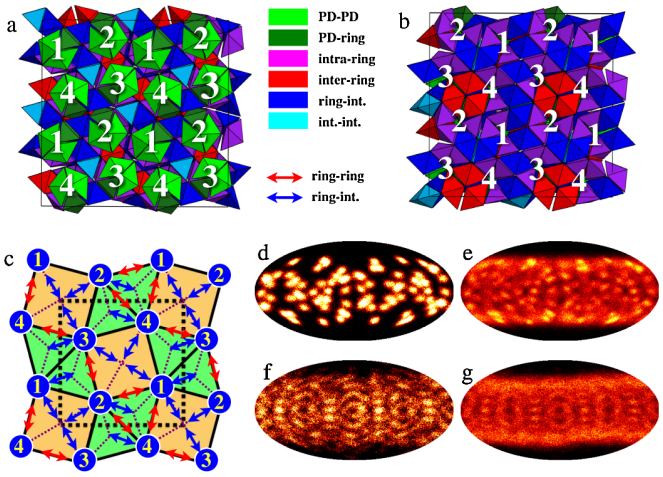

FIG. 3 (color online). (a) Top and (b) bottom views of the regular approximant. The unit cell has 41 triangular bipyramids and particles are colored according to their environment. (c) Schematics of the unit cell with connections between neighboring rings and between rings and central interstitials shown with double arrows. (d),(f) Intra-TBP and (e),(g) total bond order diagrams for (d),(e) the regular approximant and (f),(g) the degenerate approximant. In the legends, "int." stands for "interstitial."

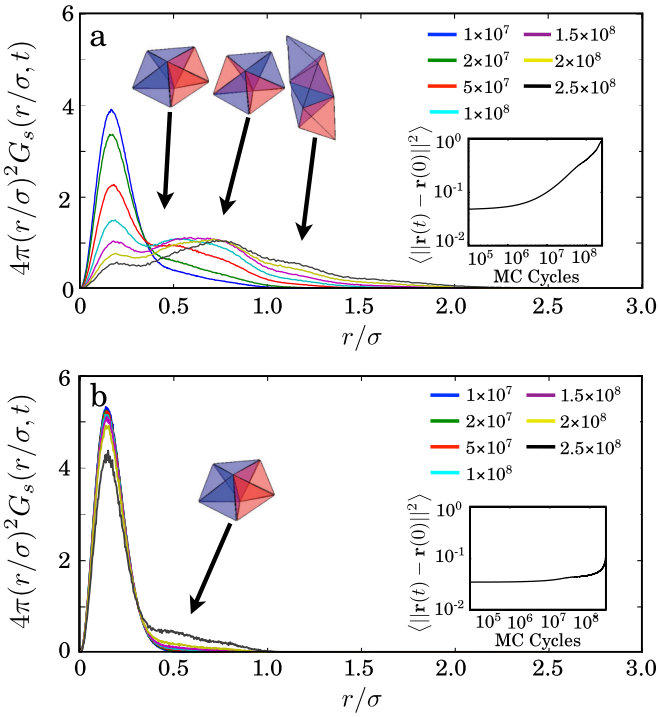

FIG. 4 (color online). The self part of the van Hove correlation function $G_s(r, t)$ measures the particle motion in the approximant. The separation distance $r(t)$ is calculated between centers of mass of member tetrahedra. (a) Large rearrangements occur at $\phi = 57\%$. (b) There is little motion present at $\phi = 60\%$. The observed dynamics is similar to that observed in the hard tetrahedron system [21].

only a small fraction of TBPs have moved as much as σ. A much faster dynamics occurs at $\phi = 57\%$. Particles at or near that density move over discrete distances that are characteristic of a PD network [Fig. 4(a)]. These rearrangements change neither the tiling nor its decoration. Instead, they reshuffle the pairing pattern by a sequence of PD rotations. After a sufficiently large number of reshuffling moves the DA emerges from the regular approximant.

Next we study the relative thermodynamic stability of various phases. We first compare the DQC obtained in simulation and its constructed approximants. As observed in Fig. 5(a), both the regular and the degenerate approximant are slightly denser than the DQC at all pressures. The relation $G(P_2^*) - G(P_1^*) \propto \int_{P_1^*}^{P_2^*} \phi^{-1} dP^*$ between the free energy and the equation of state then suggests that the approximants are thermodynamically preferred over the DQC at sufficiently high pressures because their Gibbs free energies increase more slowly with pressure. Furthermore, the approximants melt at lower pressures than the quasicrystal, which indicates that they might even be more stable than the quasicrystal at all pressures. Nevertheless, the DQC remains the only ordered phase that forms in our simulations. It is also the only structure we expect to be observed in experiments of hard nanocolloidal TBPs since the kinetic process of transforming from the DQC into the approximant is extremely slow. Considering the local structural similarity of the DQC and the fluid in terms of the PD network, the formation of the less stable DQC and not the approximant in simulation may be another example of Ostwald's rule [32].

Next, we compare the approximant with the TBP crystal by calculating the free energy difference between them.

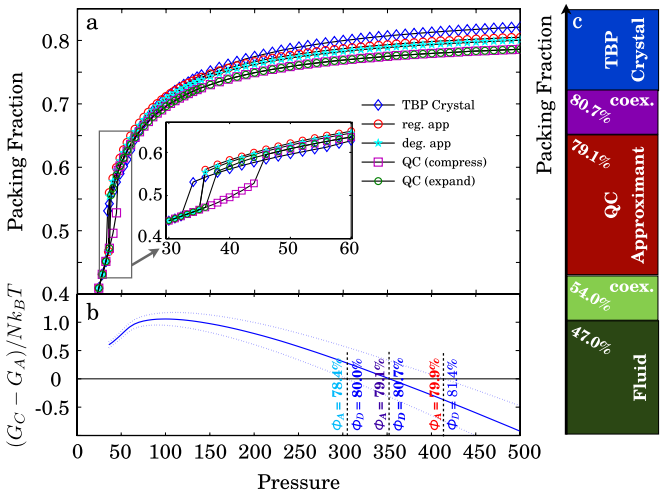

FIG. 5 (color online). (a) Equation of state for the TBP crystal, the degenerate quasicrystal, the regular and the degenerate approximants. (b) The free energy difference between the TBP crystal and the approximant. (c) Equilibrium phases of hard TBPs.

As shown in Fig. 5(b), the approximant has a lower free energy than the TBP crystal for packing fractions below 79%. A phase transition occurs at $P_c^* = 356 \pm 50$, corresponding to coexistence packing fractions of $\phi_{c,\mathrm{app}} = (79.1 \pm 0.8)\%$ and $\phi_{c,\mathrm{TBP}} = (80.7 \pm 0.7)\%$. The thermodynamic stability of the approximant at lower densities can be attributed to the additional configurational entropy associated with collective motions of particles. Such motions are not present in the TBP crystal. Their role in stabilizing the quasicrystal approximant has been shown for the structurally and dynamically similar system of hard tetrahedra [21]. The phase diagram of the hard TBP system is depicted in Fig. 5(c).

Remarkably, hard TBPs not only prefer a complex quasicrystal over the simpler TBP crystal at intermediate packing fractions, but also form it on time scales comparable to that previously observed in the hard tetrahedron system. This is surprising because, in comparison to tetrahedra, the motion of the highly anisotropic bipyramids is considerably more constrained. Nevertheless, the degeneracy of the quasicrystal helps it form easily in simulation. Random pairing allows TBPs to join existing seeds of the DQC without forming configurations that are kinetically trapped due to incorrect pairing. Particle rearrangements needed for the formation and growth of the seed are also feasible due to the local similarity of the fluid and the quasicrystal [19,33]. Finally, the degeneracy and the existence of ring-ring and ring-interstitial "cross-links" adds rigidity to the TBP structures. This means that the TBP system might be superior over the tetrahedron system in terms of its mechanical properties, just as for crystals of hard sphere dimers compared to crystals of their monomers [8].

In conclusion, we have shown that hard triangular bipyramids form a degenerate dodecagonal quasicrystal. Our finding is only the second quasicrystal formed with hard particles, the first reported degenerate quasicrystal, and one of only a few quasicrystals formed in nonatomistic systems. Our results suggest that degenerate phases are not restricted to simple close-packed crystals and might be common in dimer systems.

Resources and support for S. C. G. and A. H.-A. provided in part by the U.S. Air Force Office of Scientific Research under Multidisciplinary University Research Initiative No. FA9550-06-1-0337, subaward No. 444286-P061716. This material is based upon work also supported by the DOD/DDRE under Award No. N00244-09-1-0062 (S. C. G. and M. E.). Any opinions, findings, and conclusions or recommendations expressed in this publication are those of the author(s) and do not necessarily reflect the views of the DOD/DDRE. M. E. acknowledges support from the Deutsche Forschungsgemeinschaft. A. H.-A. acknowledges support from the University of Michigan Rackham Predoctoral Fellowship Program.

*sglotzer@umich.edu

[1] K. W. Wojciechowski, D. Frenkel, and A. C. Brańka, Phys. Rev. Lett. **66**, 3168 (1991).

[2] C. Vega, E. P. A. Paras, and P. A. Monson, J. Chem. Phys. **96**, 9060 (1992).

[3] A. P. Malanoski and P. A. Monson, J. Chem. Phys. **107**, 6899 (1997).

[4] M. Marechal and M. Dijkstra, Phys. Rev. E **77**, 061405 (2008).

[5] M. O. Blunt, J. C. Russel, M. del Carmen Jimenew-Lopez, J. P. Garrahan, X. Lin, M. Schroder, N. R. Champness, and P. H. Beton, Science **322**, 1077 (2008).

[6] S. J. Gerbode, S. H. Lee, C. M. Liddell, and I. Cohen, Phys. Rev. Lett. **101**, 058302 (2008).

[7] S. J. Gerbode, U. Agarwal, D. C. Ong, C. M. Liddell, F. Escobedo, and I. Cohen, Phys. Rev. Lett. **105**, 078301 (2010).

[8] K. V. Tretiakov and K. W. Wojciechowiski, J. Non-Cryst. Solids **352**, 4221 (2006).

[9] N. C. Karayiannis, K. Foteinopoulou, and M. Laso, Phys. Rev. Lett. **103**, 045703 (2009).

[10] N. C. Karayiannis, K. Foteinopoulou, C. F. Abrams, and M. Laso, Soft Matter **6**, 2160 (2010).

[11] B. S. John, C. Juhlin, and F. A. Escobedo, J. Chem. Phys. **128**, 044909 (2008).

[12] S. Torquato and Y. Jiao, Nature (London) **460**, 876 (2009).

[13] B. J. Wiley, Y. Xiong, Z.-Y. Li, Y. Yin, and Y. Xia, Nano Lett. **6**, 765 (2006).

[14] X. Tang, M. Tsuji, M. Nishio, and P. Jiang, Bull. Chem. Soc. Jpn. **82**, 1304 (2009).

[15] J. Zhang, S. Li, J. Wu, G. C. Schatz, and C. A. Mirkin, Angew. Chem., Int. Ed. **48**, 7787 (2009).

[16] J. Zhang, M. R. Langille, and C. A. Mirkin, J. Am. Chem. Soc. **132**, 12502 (2010).

[17] E. R. Chen, M. Engel, and S. C. Glotzer, Discrete Comput. Geom. **44**, 253 (2010).

[18] Y. Kallus, V. Elser, and S. Gravel, Discrete Comput. Geom. **44**, 245 (2010).

[19] A. Haji-Akbari, M. Engel, A. S. Keys, X. Y. Zheng, R. Petschek, P. Palffy-Muhoray, and S. C. Glotzer, Nature (London) **462**, 773 (2009).

[20] M. Oxborrow and C. L. Henley, Phys. Rev. B **48**, 6966 (1993).

[21] A. Haji-Akbari, M. Engel, and S. Glotzer, arXiv:1106.4765 [J. Chem. Phys. (to be published)].

[22] D. Levine and P. J. Steinhardt, Phys. Rev. Lett. **53**, 2477 (1984).

[23] D. Shechtman, I. Blech, D. Gratias, and J. W. Cahn, Phys. Rev. Lett. **53**, 1951 (1984).

[24] X. Zeng, G. Ungar, Y. Liu, V. Percec, S. Dulcey, and J. Hobbs, Nature (London) **428**, 157 (2004).

[25] D. V. Talapin, E. V. Shevchenko, M. I. Bodnarchuk, X. Ye, J. Chen, and C. B. Murray, Nature (London) **461**, 964 (2009).

[26] V. Elser, Phys. Rev. Lett. **54**, 1730 (1985).

[27] K. J. Strandburg, L.-H. Tang, and M. V. Jaric, Phys. Rev. Lett. **63**, 314 (1989).

[28] D. Frenkel and A. J. C. Ladd, J. Chem. Phys. **81**, 3188 (1984).

[29] See Supplemental Material at http://link.aps.org/supplemental/10.1103/PhysRevLett.107.215702 for more details.

[30] Two tetrahedra are defined as neighbors if their distance lies within the first peak of $g_t(r)$, the radial distribution function based on the centroids of the tetrahedra.

[31] A. I. Goldman and R. F. Kelton, Rev. Mod. Phys. **65**, 213 (1993).

[32] P. R. ten Wolde and D. Frenkel, Phys. Chem. Chem. Phys. **1**, 2191 (1999).

[33] A. S. Keys and S. C. Glotzer, Phys. Rev. Lett. **99**, 235503 (2007).